NATURAL CONVECTION IN SHALLOW AND TALL CAVITIES WITH THE FOUR WALLS DIFFERENTIALLY HEATED

G. Caronna, M. Corcione * and E. Habib
*Author for correspondence
Dipartimento di Fisica Tecnica, "Sapienza" University of Rome
via Eudossiana, 18 – 00184 Rome, Italy
e-mail: massimo.corcione@uniroma1.it

ABSTRACT

Steady laminar natural convection heat transfer inside air-filled rectangular cavities with differentially heated horizontal and vertical opposite walls, is studied numerically. Both cases of bottom endwall either at higher or lower temperature than the top endwall are considered. A computer code based on the SIMPLE-C algorithm is employed for the solution of the mass, momentum, and energy conservation equations. Simulations are performed for different values of the aspect ratio of the cavity from 0.25 to 4, and the Rayleigh number based on the cavity height in the range between 10^3 and 10^6, whose effects on the flow and temperature fields, and on the heat transfer rate across the enclosure, are analyzed in details.

INTRODUCTION

Most of the scientific work conducted in the past on natural convection inside rectangular enclosures has been substantially oriented to study the unidirectional heat flows which originate when the imposed heat flux or temperature difference is either simply horizontal or vertical.

Actually, much more complex boundary conditions may be encountered in practical cases, which has motivated a number of researchers to carry out studies on situations wherein a multi-directional heat flow is established across the enclosure.

This is, e.g., the case of the studies performed by: Kimura and Bejan [1], on enclosures heated from one side and cooled from below; November and Nansteel [2], and Aydin et al. [3], on enclosures heated from below and cooled at a single side, or heated at one side and cooled from the top; Ganzarolli and Milanez [4], and Basak et al. [5], on enclosures heated from below and cooled at both sidewalls; Ostrach and Raghavan [6], Shiralkar and Tien [7], and Cianfrini et al. [8], on enclosures with differentially heated horizontal and vertical opposite walls.

With specific reference to the last configuration cited above, in which a horizontal and a vertical temperature gradients are simultaneously imposed across the cavity, most of the interest has been addressed to the square geometry, mainly with the aim of evaluating the effects of either stabilizing or destabilizing vertical temperature differences on the horizontal heat transfer. In contrast, despite the importance in a number of applications, a much smaller degree of attention has been paid to the role played by the aspect ratio of the enclosure.

In this context, the aim of the present paper is to study the behavior of air-filled shallow and tall cavities, whose opposite walls are differentially heated, under the assumption that the horizontal and vertical temperature differences are the same, and that the mean temperature level of the horizontal walls is the same as that of the vertical sidewalls, which means that two adjacent walls of the enclosure are heated at same temperature T_H, while the other two walls are cooled at same temperature T_C. Both thermal configurations of bottom wall either heated or cooled with respect to the opposite top wall are examined.

The study is carried out numerically under the assumption of two-dimensional laminar flow. A computer code based on the SIMPLE-C algorithm is used for the solution of the mass, momentum and energy conservation equations. Simulations are executed for different values of the height-to-width aspect ratio of the cavity in the range between 0.25 and 4, and the Rayleigh number based on the cavity height in the range between 10^3 and 10^6, whose effects on the flow and temperature fields, as well as on the heat transfer rates, are analyzed in full detail and discussed. Dimensionless heat transfer correlating equations are also proposed.

MATHEMATICAL FORMULATION

An air-filled rectangular enclosure of height H and width L, is considered. The cavity is heated at one side, and cooled at the other side, maintained at temperatures T_H and T_C, respectively. The same temperature differential $(T_H - T_C)$ is imposed at the horizontal walls. Both cases of enclosure with bottom endwall either heated or cooled are analyzed, the former case being denoted as configuration BH, the latter as configuration BC, as sketched in Fig. 1, where the (x,y) coordinate system adopted is also represented.
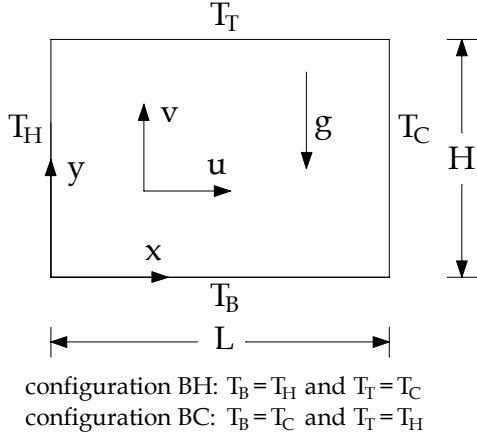
configuration BH: $T_B = T_H$ and $T_T = T_C$
configuration BC: $T_B = T_C$ and $T_T = T_H$

Figure 1 – Sketch of the geometry and coordinate system

The flow is assumed to be two-dimensional, laminar and incompressible, with constant fluid properties and negligible viscous dissipation and pressure work. The buoyancy effects on momentum transfer are taken into account by the Boussinesq approximation.

Once the above assumptions are used in the conservation equations of mass, momentum and energy, and the following dimensionless variables are introduced:

$$X = \frac{x}{H} \qquad Y = \frac{y}{H} \qquad \tau = \frac{t}{(H^2/\nu)} \tag{1}$$

$$U = \frac{u}{(\nu/H)} \qquad V = \frac{v}{(\nu/H)} \qquad P = \frac{p + \rho g y}{\rho(\nu/H)^2} \tag{2}$$

$$\theta = \frac{(T - T_C)}{(T_H - T_C)} \tag{3}$$

the following set of governing equations is obtained:

$$\frac{\partial U}{\partial X} + \frac{\partial V}{\partial Y} = 0 \tag{4}$$

$$\frac{\partial U}{\partial \tau} + U\frac{\partial U}{\partial X} + V\frac{\partial U}{\partial Y} = -\frac{\partial P}{\partial X} + \left(\frac{\partial^2 U}{\partial X^2} + \frac{\partial^2 U}{\partial Y^2}\right) \tag{5}$$

$$\frac{\partial V}{\partial \tau} + U\frac{\partial V}{\partial X} + V\frac{\partial V}{\partial Y} = -\frac{\partial P}{\partial Y} + \left(\frac{\partial^2 V}{\partial X^2} + \frac{\partial^2 V}{\partial Y^2}\right) + \frac{Ra}{Pr}\theta \tag{6}$$

$$\frac{\partial \theta}{\partial \tau} + U\frac{\partial \theta}{\partial X} + V\frac{\partial \theta}{\partial Y} = \frac{1}{Pr}\left(\frac{\partial^2 \theta}{\partial X^2} + \frac{\partial^2 \theta}{\partial Y^2}\right) \tag{7}$$

In the above equations u and v are the velocity components along x and y, respectively, i.e., horizontal and vertical; t is the time; T is the temperature; p is the pressure; ρ is the density; g is the acceleration of gravity; ν is the kinematic viscosity; Pr is the Prandtl number; and Ra is the Rayleigh number defined as:

$$Ra = \frac{g\beta(T_H - T_C)H^3}{\nu^2} Pr \tag{8}$$

The boundary conditions assumed are the no-slip condition $U = V = 0$ at the four boundary walls, and $\theta = 1$ at the heated walls and $\theta = 0$ at the cooled walls.

The initial conditions assumed are fluid at rest, i.e., $U = V = 0$, and uniform temperature $\theta = 0$ throughout the whole cavity.

COMPUTATIONAL PROCEDURE

The set of governing equations (4)–(7) with the boundary and initial conditions stated above is solved by a control-volume formulation of the finite-difference method.

The coupling of velocity and pressure is handled through the SIMPLE-C algorithm by Van Doormaal and Raithby [9]. The QUICK discretization scheme by Leonard [10] is used for the evaluation of the interface advection fluxes. A second-order backward scheme is used for time stepping. Starting from the assigned initial fields of the dependent variables across the cavity, at each time-step the discretized governing equations are solved iteratively through a line-by-line application of the Thomas algorithm, enforcing under-relaxation for convergence.

The computational spatial domain is covered with a non-uniform grid, having a concentration of grid lines near the boundary walls, and a uniform spacing across the remainder interior of the enclosure. Time discretization is chosen uniform. Within each time step, the spatial solution is considered to be fully converged when the maximum absolute values of both the mass source and the percentage changes of the dependent variables at any grid-node from iteration to iteration are smaller than the prescribed values, i.e., 10^{-4} and 10^{-5}, respectively. Time-integration is stopped once steady-state is reached. This means that the simulation procedure ends when the percentage difference between the incoming and outgoing heat transfer rates, and the percentage changes of the time-derivatives of the dependent variables at any grid-node between two consecutive time-steps, are smaller than the prescribed values, i.e., 10^{-6} and 10^{-7}, respectively.

Once steady-state is reached, the average Nusselt numbers of the heated and cooled sidewalls Nu_H and Nu_C, and those of the bottom and top endwalls Nu_B and Nu_T, are calculated:

$$Nu_H = -\int_0^1 \frac{\partial \theta}{\partial X}\bigg|_{X=0} dY \tag{9}$$

$$Nu_C = +\int_0^1 \frac{\partial \theta}{\partial X}\bigg|_{X=1/A} dY \tag{10}$$

$$Nu_B = -A\int_0^{1/A} \frac{\partial \theta}{\partial Y}\bigg|_{Y=0} dX \tag{11}$$

$$Nu_T = +A\int_0^{1/A} \frac{\partial \theta}{\partial Y}\bigg|_{Y=1} dX \tag{12}$$

where $A = H/L$ is the height-to-width aspect ratio of the cavity, and the temperature gradients are evaluated by a second-order profile among each wall-node and the next two corresponding fluid-nodes.

It is worth noticing that, for all the configurations analyzed, the centro-symmetry of the system has brought to the following results:

$$Nu_H = Nu_C \tag{13}$$

$$Nu_B = Nu_T \tag{14}$$

which means that whatever heat is transferred to the fluid at the heated sidewall, the same amount of heat is withdrawn from the fluid at the opposite cooled sidewall; a similar situation exists for the horizontal walls. This implies that, at steady-state, the Nusselt numbers Nu_H and Nu_C may be interpreted as the average Nusselt number across the cavity along the x-direction, i.e., the horizontal average Nusselt number Nu_h, while the Nusselt numbers Nu_B and Nu_T represent the vertical average Nusselt number Nu_v:

$$Nu_h = Nu_H = Nu_C \tag{15}$$

$$Nu_v = Nu_B = Nu_T \tag{16}$$

The overall thermal performance of the enclosure is then expressed in terms of the average Nusselt number Nu of the whole cavity, which is calculated as:

$$Nu = \frac{Nu_h + (1/A)Nu_v}{1 + (1/A)} \tag{17}$$

Tests on the dependence of the results on both grid-size and time-step have been performed for several combinations of A and Ra, for both configurations BH and BC. The optimal grid-size and time-step used for computations, representing a good compromise between solution accuracy and computational time required, are such that further refinements do not yield for any noticeable modification neither in the heat transfer rates nor in the flow field at steady-state, that is, the percentage changes of Nu_h and Nu_v, as well as those of the maximum horizontal and vertical velocity components U and V on the two midplanes of the enclosure, are smaller than the prescribed accuracy values, i.e., 1% and 2%, respectively. Typically, the number of nodal points and the time stepping used for computations lie in the ranges between 40×40 and 80×400, and between 10^{-6} and 10^{-3}, respectively.

Moreover, some test runs have also been executed with the initial uniform dimensionless temperature of the fluid set to 0.5 or 1, in order to determine the effect of the initial conditions on the steady-state flow and temperature fields. Indeed, solutions practically identical to those obtained for $\theta = 0$ were obtained for all the configurations examined.

Finally, in order to validate the numerical code used for the present study, the steady-state solutions obtained for $\tau \to \infty$ in a square cavity with differentially heated sidewalls and adiabatic top and bottom endwalls for Rayleigh numbers from 10^3 to 10^6, have been compared with the benchmark data of de Vahl Davis [11]. In particular, the average Nusselt numbers as well as the maximum horizontal and vertical velocity components, on the vertical and horizontal midplanes, respectively, are well within 1% of the benchmark data, as reported in Table 1. It is worth noticing that our dimensionless velocity results have been

multiplied by the Prandtl number before being inserted in Table 1, so as to account for the choice of the ratio between kinematic viscosity and characteristic length of the cavity as scale factor for the velocity, instead of the ratio between thermal diffusivity and characteristic length, used in ref. [11]. More details on the code validation are available in Cappelli D'Orazio et al. [12].

Table 1 – Comparison of thermally-driven square cavity solutions

Ra		U_{max}	V_{max}	Nu_{av}
10^3	Present	3.654	3.708	1.116
	Benchmark [11]	3.649	3.697	1.118
10^4	Present	16.242	19.714	2.254
	Benchmark [11]	16.178	19.617	2.243
10^5	Present	35.008	68.109	4.506
	Benchmark [11]	34.722	68.590	4.519
10^6	Present	65.226	221.598	8.879
	Benchmark [11]	64.630	219.360	8.800

RESULTS AND DISCUSSION

Numerical simulations are performed for Pr = 0.71, which corresponds to air, and different values of the height-to-width aspect ratio of the enclosure in the range between 0.25 and 4, and the Rayleigh number of the cavity in the range between 10^3 and 10^6, for both configurations BH and BC.

A selection of local results is presented in Figs. 2−7 and in Figs. 8−13 for configurations BH and BC, respectively. In these figures, isotherms and streamlines are plotted for different sets of values of A and Ra, in order to highlight the effects of any independent parameter on the temperature and flow fields.

In the isotherm plots, the contours correspond to equispaced values of the dimensionless temperature θ in the range between 0 and 1. In the streamline plots, the contours correspond to equispaced values of the normalized dimensionless stream function $|\Psi|/|\Psi|_{max}$ in the range between 0 and 1, where Ψ is defined as usual through U=∂Ψ/∂Y and V=−∂Ψ/∂X. The values of $|\Psi|_{max}$ for different combinations of values of A and Ra, for both configurations BH and BC, are reported in Table 2.

Table 2 – Values of $|\Psi|_{max}$ for different combinations of A and Ra, in both cases of heating from below and heating from above

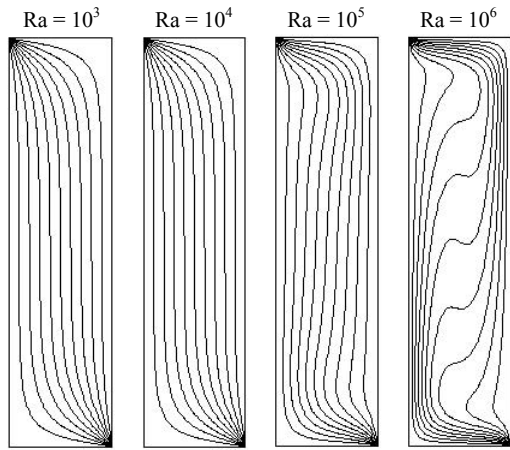| Ra	config.	$|\psi|_{max}$				
		A = 0.25	0.5	1	2	4
10^3	BH	1.16	1.01	1.59	0.42	0.05
	BC	0.71	0.81	1.21	0.41	0.05
10^4	BH	25.23	13.06	11.40	4.18	0.55
	BC	3.80	4.51	5.50	3.49	0.55
10^5	BH	86.81	45.85	35.96	19.61	5.49
	BC	11.72	11.93	12.02	13.33	5.30
10^6	BH	246.30	128.40	61.88	44.57	29.12
	BC	25.64	23.88	22.63	21.87	25.15

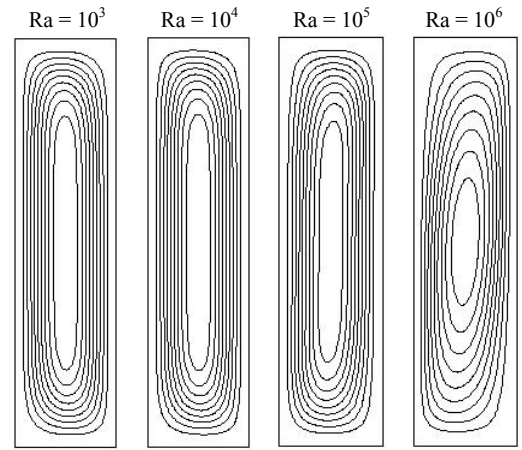**Figure 2** – Isotherms of BH model for A = 4 and Ra = 10^3–10^6

Figure 5 – Streamlines of BH model for A = 4 and Ra = 10^3–10^6
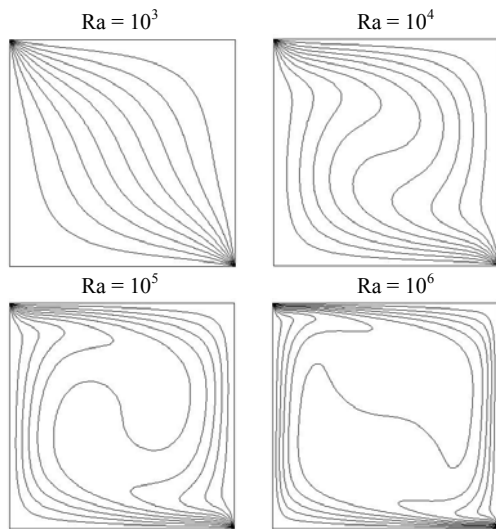

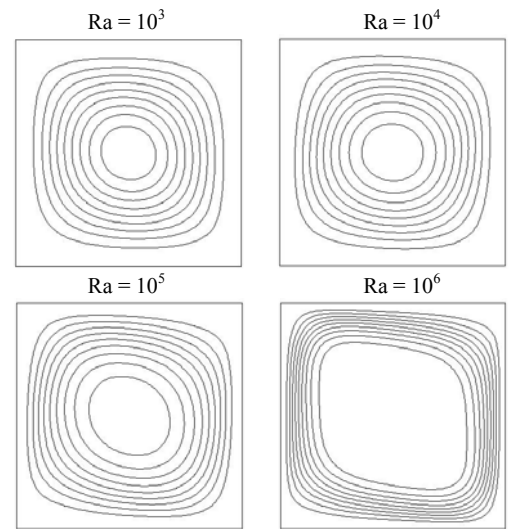**Figure 3** – Isotherms of BH model for A = 1 and Ra = 10^3–10^6

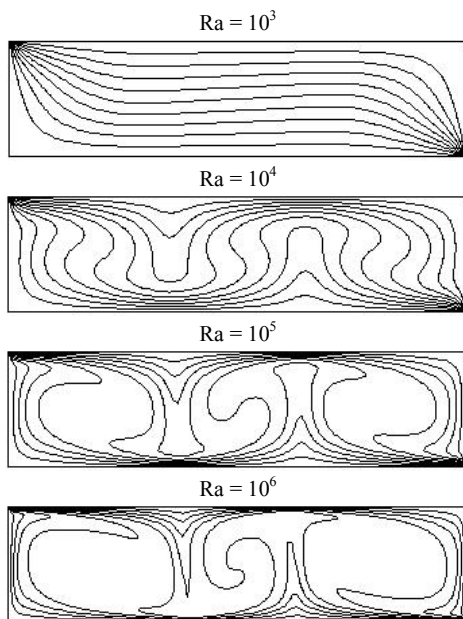**Figure 6** – Streamlines of BH model for A = 1 and Ra = 10^3–10^6

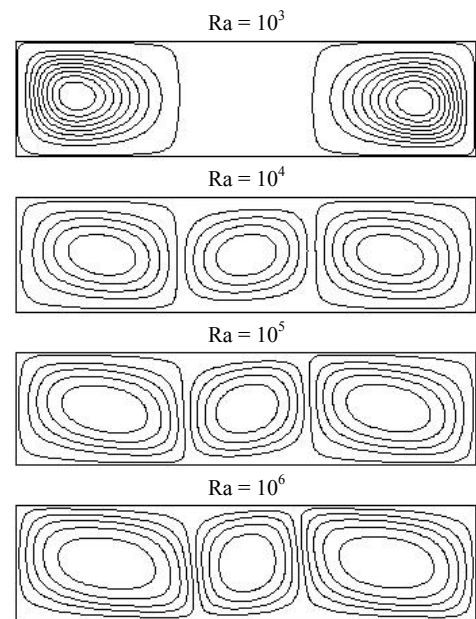**Figure 4** – Isotherms of BH model for A = 0.25 and Ra = 10^3–10^6

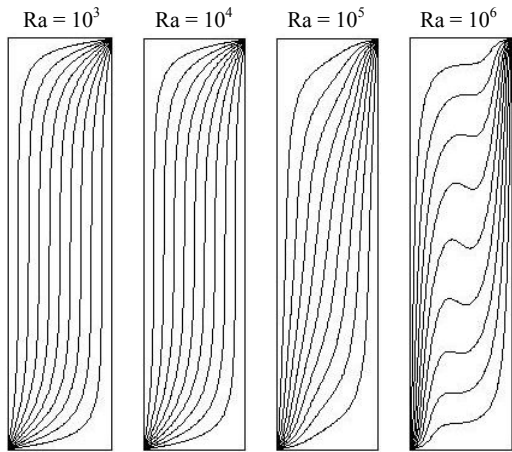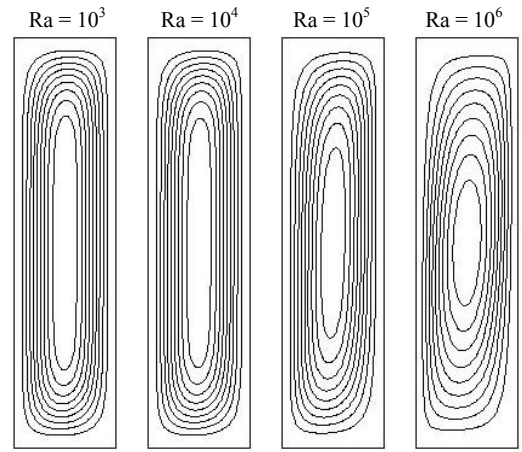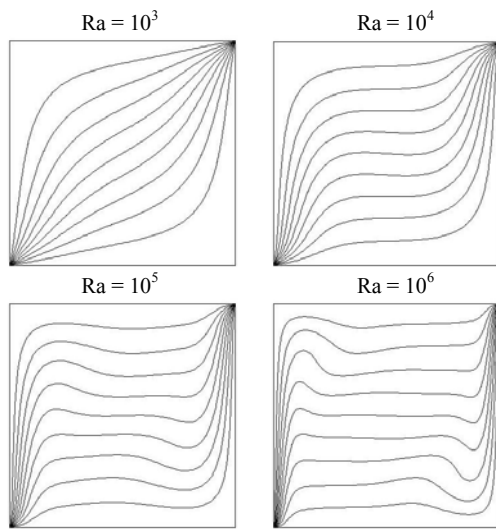**Figure 7** – Streamlines of BH model for A = 0.25 and Ra = 10^3–10^6

Figure 8 – Isotherms of BC model for A = 4 and Ra = 10^3–10^6

Figure 11 – Streamlines of BC model for A = 4 and Ra = 10^3–10^6

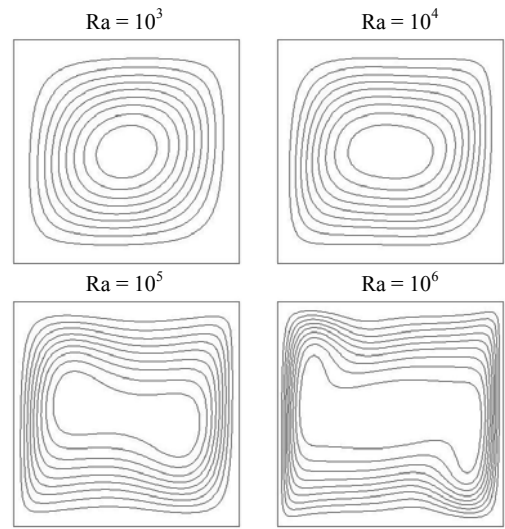

Figure 9 – Isotherms of BC model for A = 1 and Ra = 10^3–10^6

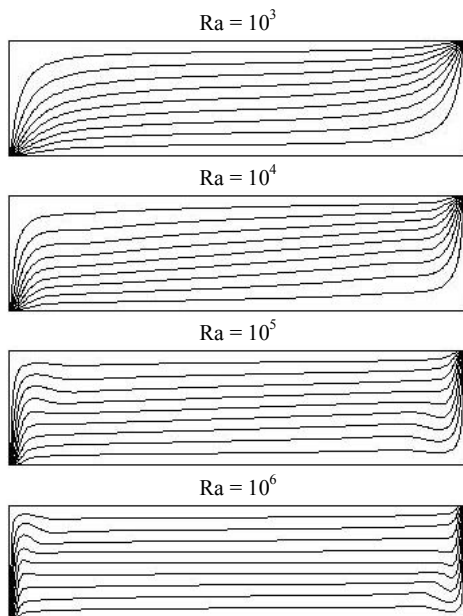**Figure 12** – Streamlines of BC model for A = 1 and Ra = 10^3–10^6

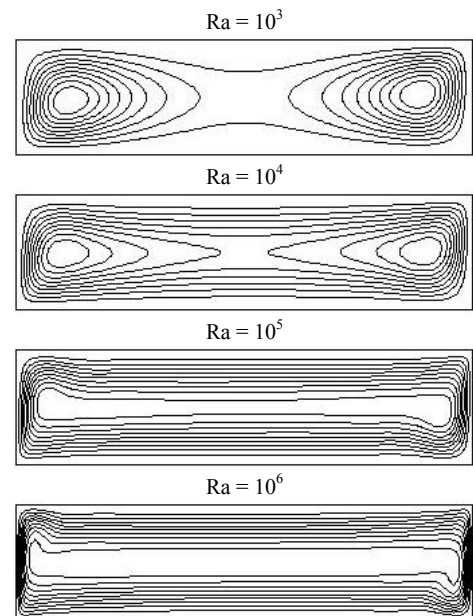**Figure 10** – Isotherms of BC model for A = 0.25 and Ra = 10^3–10^6

Figure 13 – Streamlines of BC model for A = 0.25 and Ra = 10^3–10^6
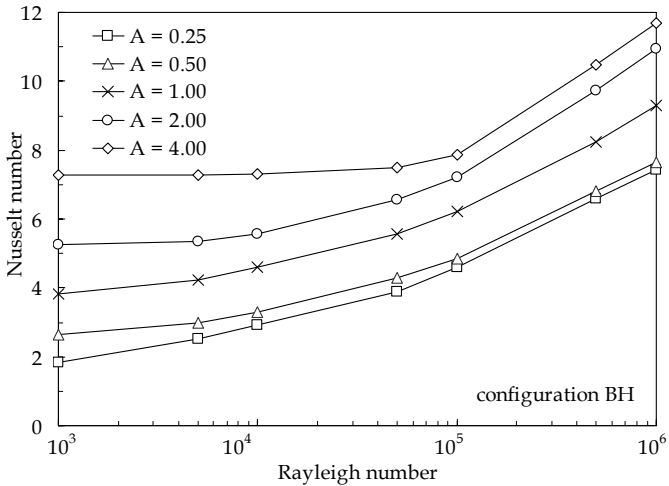
Figure 14 – Distributions of Nu vs. Ra for different values of A in the range between 0.25 and 4 (configuration BH)
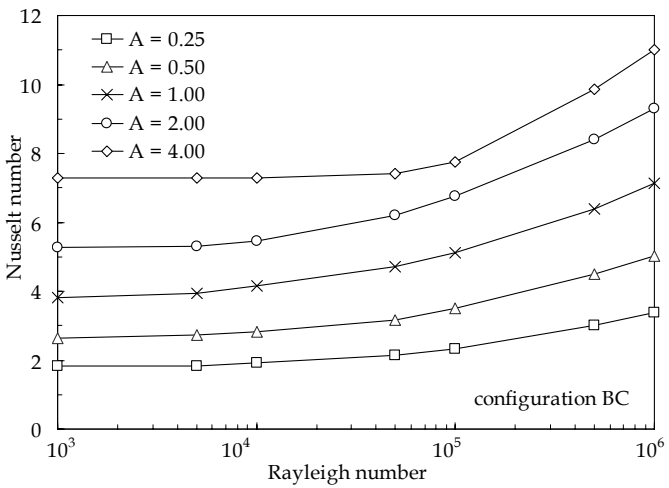

Figure 15 – Distributions of Nu vs. Ra for different values of A in the range between 0.25 and 4 (configuration BC)
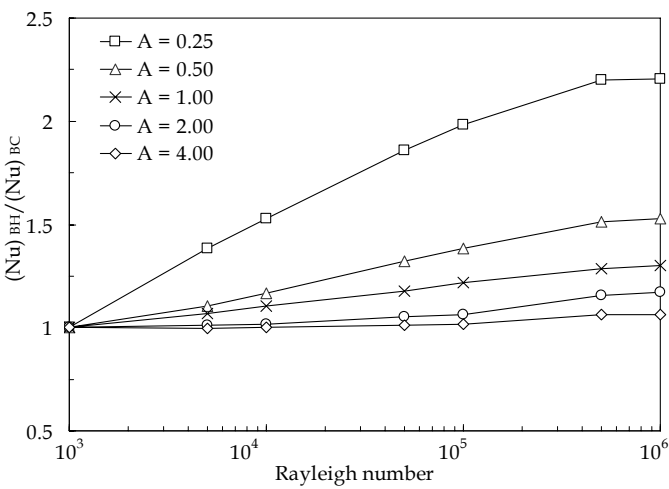

Figure 16 – Distributions of the ratio between the Nusselt numbers for configurations BH and BC vs. Ra for different values of A

It is worth noticing that the effect of the geometry of the cavity on the intensity of the fluid motion (which obviously increases as the Rayleigh number increases) is quite different according as the cavity is heated from below or from above, as shown in Table 2. As regards configuration BH, a remarkable increase in the rate of the fluid circulation occurs as the cavity aspect ratio A decreases. In fact, the upward-imposed vertical temperature gradient has a significant destabilizing effect on the temperature and velocity fields which would establish inside the enclosure if only the horizontal temperature gradient were applied, thus preventing the formation of the vertical thermal stratification typical of enclosures with differentially heated sides and perfectly insulated top and bottom walls. However, such effect is definitely more pronounced for shallow rather than for slender geometries. In contrast, for configuration BC the effect of the aspect ratio on the circulation rate inside the enclosure is smaller, since the downward-imposed temperature gradient has a stabilizing effect, which induces a well defined vertical stratification across the cavity, whatever is its geometry. Of course, the facts discussed above are clearly reflected by the isotherm and streamline patterns depicted in Figs. 2–13.

As far as the heat transfer performance of the enclosure is concerned, the distributions of the average Nusselt number Nu of the whole cavity vs. the Rayleigh number for different values of the aspect ratio of the enclosure are plotted in Figs. 14 and 15, for configurations BH and BC, respectively. Moreover, the distributions of the ratio $(Nu)_{BH}/(Nu)_{BC}$ between the average Nusselt numbers for configurations BH and BC vs. Ra are plotted in Fig. 16 for different values of A. It may be noticed that the different types of heating condition considered, either from below or from above, have a significant effect on the heat transfer rate across the enclosure only for square and shallow cavities, due to the larger thermal contribution of the horizontal walls to the fluid motion. This may be clearly put in evidence by comparing Figs. 2 and 8, for A = 4, and Figs. 4 and 10 for A = 0.25. It may be observed that for A = 4 the isotherms have patterns not too different, with a weak vertical stratification in the middle of the cavity, whereas for A = 0.25 their distributions are completely different. In fact, in such case the heating from above produces a strongly stratified field, thus implying that, leaving aside the layers adjacent to both sidewalls, conduction is the dominat mode of heat transfer across the enclosure. In contrast, the heating from below produces the breakdown of such density stratification, which brings to the formation of a multi-cellular flow structure.

The results obtained for the average Nusselt number Nu, for both heating configurations BH and BC, may be expressed as a function of the independent variables Ra and A through the following dimensionless correlating-equations:

<u>configuration BH – heating from below</u>

$$Nu = [(3.6A^{0.5})^5 + (0.54A^{0.183}Ra^{0.206})^5]^{1/5} \tag{18}$$

<u>configuration BC – heating from above</u>

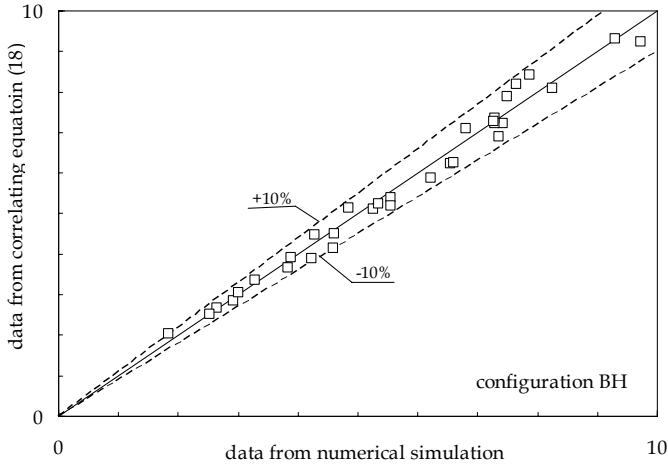$$Nu = [(3.6A^{0.5})^5 + (0.60A^{0.435}Ra^{0.172})^5]^{1/5} \tag{19}$$

Figure 17 – Comparison between the Nusselt numbers predicted by equation (18) and those derived from the numerical simulations.
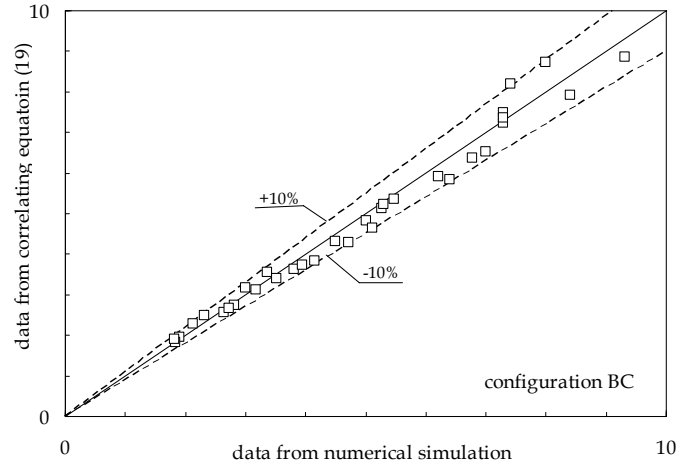

Figure 18 – Comparison between the Nusselt numbers predicted by equation (19) and those derived from the numerical simulations.

for $0.25 \leq A \leq 4$ and $10^3 \leq Ra \leq 10^6$, both with a $\cong 5\%$ standard deviation of error and a $\pm 10\%$ range of error, as shown in Figs. 17 and 18.

CONCLUSIONS

Steady laminar natural convection heat transfer inside air-filled rectangular cavities with differentially heated horizontal and vertical opposite walls, has been studied numerically. Both cases of heating from the bottom and from the top, denoted as configurations BH and BC, respectively, have been considered. Simulations have been performed for different values of the height-to-width aspect ratio of the cavity in the range between 0.25 and 4, and the Rayleigh number based on the height of the cavity in the range between 10^3 and 10^6.

It has been found that the heat transfer performance of the cavity increases with increasing the Rayleigh number and the aspect ratio. In addition, the two types of heating condition considered, either from below or from above, have a significant effect on the amount of heat transferred across the cavity only for square and shallow geometries. In particular, for the shallow cavity with aspect ratio $A = 0.25$ at $Ra = 10^5$–10^6, the average Nusselt number of configuration BH is more than the double than that of configuration BC, whereas for the tall cavity with aspect ratio $A = 4$ such Nusselt numbers are practically the same, even at the largest Rayleigh number investigated.

NOMENCLATURE

A   height-to-width aspect ratio of the enclosure
g   gravitational acceleration
H   height of the enclosure
L   width of the enclosure
Nu   average Nusselt number
P   dimensionless pressure
p   pressure
Pr   Prandtl number = ν/α
Ra   Rayleigh number = $g\beta(T_H - T_C)H^3 Pr/\nu^2$
T   temperature

t   time
U   dimensionless horizontal velocity component
u   horizontal velocity component
V   dimensionless vertical velocity component
v   vertical velocity component
X   dimensionless horizontal coordinate
x   horizontal coordinate
Y   dimensionless vertical coordinate
y   vertical coordinate

Greek symbols
α thermal diffusivity of the fluid
β coefficient of volumetric thermal expansion of the fluid
ν kinematic viscosity of the fluid
θ dimensionless temperature
ρ density of the fluid
τ dimensionless time
ψ dimensionless stream function

Subscripts
B   bottom
C   cold
H   hot
h   horizontal
max   maximum value
T   top
v   vertical

REFERENCES

[1] S. Kimura, A. Bejan, Natural convection in a differentially heated corner region, Phys. Fluids 28 (1985) 2980-2989.
[2] M. November, M. W. Nansteel, Natural convection in rectangular enclosures heated from below and cooled along one side, Int. J. Heat Mass Transfer 30 (1987) 2433-2440.
[3] O. Aydin, A. Unal, T. Ayhan, Natural convection in rectangular enclosures heated from one side and cooled

from the ceiling, Int. J. Heat Mass Transfer 42 (1999) 2345-2355.

[4] M. M. Ganzarolli, L. F. Milanez, Natural convection in rectangular enclosures heated from below and symmetrically cooled from the sides, Int. J. Heat Mass Transfer 38 (1995) 1063-1073.

[5] T. Basak, S. Roy, A. R. Balakrishnan, Effects of thermal boundary conditions on natural convection flows within a square cavity, Int. J. Heat Mass Transfer 49 (2006) 4525-4535.

[6] S. Ostrach, C. Raghavan, Effect of stabilizing thermal gradients on natural convection in rectangular enclosures, J. Heat Transfer 101 (1979) 238-243.

[7] G. S. Shiralkar, L. Tien, A numerical study of the effect of a vertical temperature difference imposed on a horizontal enclosure, Num. Heat Transfer 5 (1982) 185-197.

[8] C. Cianfrini, M. Corcione, P. P. Dell'Omo, Natural convection in tilted square cavities with differentially heated opposite walls, Int. J. Thermal Sciences 44 (2005) 441-451.

[9] J. P. Van Doormaal and G. D. Raithby, Enhancements of the simple method for predicting incompressible fluid flows, Num. Heat Transfer 11 (1984) 147-163.

[10] B. P. Leonard, A stable and accurate convective modelling procedure based on quadratic upstream interpolation, Comp. Meth. in Appl. Mech. Engng. 19 (1979) 59-78.

[11] G. de Vahl Davis, Natural convection of air in a square cavity: a bench mark numerical solution, Int. J. Num. Meth. Fluids 3 (1983) 249–264.

[12] M. Cappelli D'Orazio, C. Cianfrini, M. Corcione, Rayleigh-Bénard convection in tall rectangular enclosures, Int. J. Thermal Sciences 43 (2004) 135-144.